chemosensors

MDPI

Article

Creatinine Sensing with Reduced Graphene Oxide-Based Field Effect Transistors

Melody L. Candia, Esteban Piccinini, Omar Azzaroni * and Waldemar A. Marmisollé *

Department of Chemistry, Faculty of Exact Sciences, Institute of Theoretical and Applied Physical and Chemical Research (INIFTA), National University of La Plata (UNLP), CONICET. 64 and 113, La Plata B1900, Argentina; melodycandia@inifta.unlp.edu.ar (M.L.C.); estebanpiccinini@inifta.unlp.edu.ar (E.P.)
* Correspondence: azzaroni@inifta.unlp.edu.ar (O.A.); wmarmi@inifta.unlp.edu.ar (W.A.M.)

Abstract

Creatinine (Crn) is a clinically relevant biomarker commonly used for the diagnosis and monitoring of kidney disease. In this work, we report the fabrication of reduced-graphene-oxide-based field-effect transistors (rGO FETs) for Crn detection. These devices were functionalized using a layer-by-layer (LbL) assembly, in which polyethyleneimine (PEI) and creatinine deiminase (CD) were alternately deposited. This LbL strategy allows for the effective incorporation of CD without compromising its structural or functional integrity, while also taking advantage of the local pH changes caused by creatinine hydrolysis. It also benefits from the use of a polyelectrolyte that can amplify the enzymatic signal. Furthermore, it enables scalable and efficient fabrication. These transistors also address the challenges of point-of-care implementation in single-use cartridges. It is worth noting that the devices showed a linear relationship between the Dirac-point shift and the logarithm of the creatinine concentration in the 20–500 μM range in diluted simulated urine. The sensor response improved with increasing numbers of PEI/CD bilayers. Furthermore, the functionalized FETs demonstrated rapid detection dynamics and good long-term stability. Present results confirm the potential of these devices as practical biosensors for sample analysis under real-world conditions, making them ideal for implementation in practical settings.

Keywords: creatinine; rGO FETs; creatinine deiminase

1. Introduction

Creatinine is the second most studied biomarker in the clinical field, after glucose [1]. It is a product of creatine metabolism that is transported by the bloodstream, filtered by the kidneys and finally excreted in the urine [2]. Its concentration in urine typically ranges from 4.4 to 18 mM in a healthy individuals [3]. Values outside this range are indicative of kidney diseases or muscular and cardiovascular disorders [2]. Regarding chronic kidney disease, which has a global prevalence of approximately 10%, the measurement of creatinine in urine and blood enables the estimation of key indicators used to diagnose and stratify the disease [4]. Chronic kidney disease (CKD) is characterized by a decline in kidney function, indicated by a glomerular filtration rate (GFR) of less than 60 mL·min^{-1} per 1.73 m^2 [5]. CKD eventually leads to end-stage renal disease, where the treatment options are kidney transplantation or dialysis, the latter being the most common. However, it is associated with a lower quality of life, high medical costs, and a high mortality rate, highlighting the importance of early CKD detection. Creatinine is one of the biomarkers used for the

Check for updates

Received: 22 October 2025
Revised: 8 December 2025
Accepted: 18 December 2025
Published: 20 December 2025

Copyright: © 2025 by the authors. Licensee MDPI, Basel, Switzerland. This article is an open access article distributed under the terms and conditions of the Creative Commons Attribution (CC BY) license.

detection and monitoring of kidney disease. Since the urinary creatinine measurement is required to determine the albumin-to-creatinine ratio (ACR), whereas serum creatinine assessment is essential for the estimation of glomerular filtration rate (GFR). The Jaffe reaction is the most widely used method to determine creatinine concentration in urine [1]. Spectrophotometric methods derived from it tend to have high detection limits and are easily affected by interfering species. Other methods such as high-performance liquid chromatography (HPLC), mass spectrometry (MS) and electrochemistry, have demonstrated high sensitivity and reproducibility [6–9]. However, they require sophisticated, expensive, and high-volume instruments, as well as long analysis times. This highlights the need for new detection techniques for creatinine sensing. One alternative to address these limitations is the use of enzymatic detection systems, which leverage the inherent selectivity of enzymes. Commonly known as point-of-care (POC) tests [1,10–12], they are generally used in clinical trials due to their real-time measurements, selectivity, sensitivity, speed, and ease of use.

Field-effect transistors offer several inherent advantages as sensing devices, making them particularly suitable for detecting small biochemical perturbations such as the local pH changes generated by enzymatic activity. First, FETs provide intrinsic signal amplification: small variations in the effective gate potential or channel conductance—arising from interfacial charge redistribution or pH modulation—translate into measurable changes in the channel conductance, often with higher sensitivity than purely potentiometric methods. Second, FET signals are directly electrical and readily digitizable, enabling fast, real-time readout without the need for additional transduction steps. Third, FET architectures are compatible with miniaturization and scalable fabrication, which facilitates device integration, multiplexing, and ultimately the development of compact platforms for rapid biochemical sensing [13,14]. In this context, reduced graphene oxide-based FETs (rGO FETs) have proven to be an excellent candidate for monitoring pH changes caused by enzymatic reactions [15,16]. This sensitivity to pH changes is due to the presence of remaining functional groups, such as -OH and -COOH, on the surface of reduced graphene oxide (rGO). These functional groups can alter the charge of the graphene surface and modify the diffuse double layer, giving rise to gating effects [15,17–19]. These properties demonstrate the high potential of rGO FETs for the development of pH-sensitive sensors. Moreover, graphene is a two-dimensional semiconductor material with good chemical stability, high conductivity, high carrier mobility, and large specific area [20–22]. Furthermore, these rGO FETs are capable of performing measurements with minimal sample volumes [23]. Due to these properties, these devices are promising for the development of bioelectronic transducers. In this regard, rGO FETs have enabled the detection of ions and charged biomolecules without the need for labels, with high sensitivity and in real time [24–26]. Their operation is supported on the fact that the conductivity of the semiconductor channel (rGO) between the drain and source electrodes can be modulated by applying a potential difference between the gate and source electrodes (V_G). The application of this V_G potential affects the current between the drain and source electrodes (I_{DS}) since it produces a change in the charge carriers density of rGO. The point at which the conductivity is minimum is known as the Dirac point (V_i). For graphene, this corresponds to the state at which the conductance band is completely unoccupied and the valence band is full [27,28].

The characteristics of the interfacial architecture and the immobilization of the recognition elements will determine the performance of the biosensors. In this sense, the integration of different recognition elements in graphene transistors such as antibodies, ionophores, aptamers and enzymes, has emerged as promising tools in the fabrication of biosensors [16,29,30]. After immobilizing these recognition elements on the graphene surface, their activity must be preserved and access to their active sites must be allowed. In

this context, one of the most used immobilization techniques for biomolecules in graphene transistors is through covalent bonding, but one of its drawbacks is that it could alter the functionality of the recognition biomolecule if essential groups are involved in the immobilization [31]. Likewise, it can introduce defects into the sp^2 carbon network of graphene, affecting charge transport and, consequently, the sensor response [32,33]. A versatile and simple alternative to overcome these issues is the layer-by-layer (LbL) assembly technique, which involves sequential deposition of oppositely charged species through electrostatic interactions [16,34]. In particular, the integration of enzymes in LbL assemblies is a strategy to immobilize recognition elements without altering their structural and functional properties [35]. In this configuration, enzymatic activity can generate local pH changes that alter the charge in the remaining groups of the graphene surface, altering the response to a V_G potential and its conductivity. Furthermore, it has been reported that incorporating a weak polyelectrolyte, as polyethyleneimine (PEI), into the LbL assembly enhances pH sensitivity by introducing additional ionizable groups [19,36]. Thus, the local pH changes generated by the enzymatic reaction can alter the charge of the polyelectrolyte causing an amplification of the charge change on the graphene surface [19,37].

Considering the advantages of rGO FETs and the need to develop new biosensing devices, in this work we present the development of biosensors for creatinine detection using rGO FETs functionalized using the LbL strategy. Particularly, PEI and creatinine deiminase (CD) were alternately deposited. As mentioned above, this LbL strategy allowed for the immobilization of CD while preserving its structural and functional properties, in addition to taking advantage of the local pH changes caused by creatinine hydrolysis [38]. These PEI/CD-functionalized rGO FETs exhibited a shift in the Dirac potential upon exposure to creatinine, resulting from local pH changes on the graphene surface. The magnitude of this shift was observed to correlate with the analyte concentration.

Previous studies have demonstrated that PEI–enzyme multilayers assembled on graphene and rGO FETs can serve as functional biosensing platforms, particularly for urea detection using urease–PEI films and for cascade reactions combining urease and arginase [19,36]. However, these studies relied on chronoamperometric operation under continuous flow, where the analytical signal was extracted from the time-dependent evolution of the drain current at a fixed gate potential. In contrast, the approach developed in the present work operates entirely under static conditions and is based on the acquisition of full I_{DS}–V_G transfer curves at each analyte concentration. This measurement strategy not only eliminates the need for flow cells or injection systems but also provides access to richer electrical information. Although in this study we focus on the Dirac point shift as the primary analytical parameter, the availability of complete transfer characteristics enables future implementation of multiparametric analysis, which may enhance the sensitivity [39] and robustness of FET-based sensing strategies [40]. Furthermore, the biosensors based on PEI/CD LbL assemblies demonstrated rapid detection dynamics and good long-term stability.

2. Materials and Methods

2.1. Reagents

The following reagents and chemicals were used: creatinine deiminase (III) (13.3 U/mg, Sorachim, Lausanne, Switzerland), creatinine anhydrous (≥98%, Sigma-Aldrich, Darmstadt, Germany), sodium 1-pyrenesulfonate (97%, Sigma, Darmstadt, Germany), dimethylformamide (Biopack, Buenos Aires, Argentina), poly(ethylenimine) solution (50% in water, average MW ~10,000, Sigma, Darmstadt, Germany), potassium phosphate monobasic (Cicarelli, San Lorenzo, Santa Fe, Argentina), sodium carbonate (Anedra, Los Troncos del Talar, Buenos Aires, Argentina), urea (Biopack, Buenos Aires, Argentina), potassium chloride (Anedra, Los Troncos del Talar, Buenos Aires, Argentina) and HEPES (Anedra, Los

Troncos del Talar, Buenos Aires, Argentina), PDADMAC (poly(diallyldimethylammonium chloride, 20% in H_2O, average MW ~100,000−200,000, Sigma-Aldrich, St. Louis, MO, USA) and PSS (poly(sodium 4-styrenesulfonate), average MW ~1,000,000, Sigma-Aldrich, St. Louis, MO, USA).

2.2. Measurement Set-Up

Electrical measurements were carried out using rGO FETs containing rGO sheets deposited on interdigitated gold microelectrodes as source and drain electrodes, and a coplanar Ag/AgCl microelectrode was used as the gate electrode were supplied by GISENS BIOTECH (Berkeley, CA, USA). The rGO FETs featured a 10 µm channel length and a 55.2 mm channel width, together with a coplanar Ag gate that was chemically oxidized to form Ag/AgCl. Electrical measurements were performed using a TEQ bipotentiostat (NanoTeq, Buenos Aires, Argentina) and an electrochemical bath cell (Micrux instruments) to confine the detection solution to the chamber area of the rGO FET.

To determine the rGO FETs response, the drain-source current (I_{DS}) was measured as a function of the gate potential (characteristic curves, I_{DS}–V_G) using a constant V_{DS} of 50 mV. The V_G was scanned at 10 mV s^{-1}.

2.3. Layer-by-Layer (LbL) Modification of the Graphene Semiconductor Channel

The rGO channel functionalization was performed as previously described [19]. Briefly, rGO FETs were incubated overnight in 5 mM sodium 1-pyrenesulfonate (SPS) in dimethylformamide (DMF), subsequently rinsed three times with DMF and with deionized water. They were then incubated for 10 min in an aqueous solution of 2 mg/mL polyethyleneimine (PEI) at pH 8.5 and rinsed with deionized water. They were subsequently incubated for 30 min in a solution of 1 mg/mL creatinine deiminase (CD) in 0.1 mM HEPES buffer and 10 mM KCl at pH 7.4 and subsequently rinsed with deionized water. The LbL assembly was fabricated by alternating the deposition of a weak polyelectrolyte, PEI (a polycation), and CD (negatively charged at pH 7.4). This deposition process, alternating between the polyelectrolyte and the enzyme, was repeated as needed to incorporate the desired number of layers.

2.4. Improved Structural Stability

To improve the structural stability of the LbL on the rGO FETs $(PEI\text{-}CD)_3$, these assemblies were further covered with a protective coating of $(PDADMAC/PSS)_3$. The rGO FETs $(PEI/CD)_3$ were incubated for 10 min in a 1 mg/mL PDADMAC 10 mM KCl solution, washed with Milli-Q water, and subsequently incubated in a 1 mg/mL PSS 10 mM KCl solution. This alternating deposition process was repeated two more times to achieve a three-bilayer protective coating, $(PDADMAC/PSS)_3$. Thus, the rGO FETs $(PEI/CD)_3$ $(PDADMAC/PSS)_3$ were obtained.

2.5. Surface Plasmon Resonance (SPR) Spectroscopy

To monitor LbL assembly, a multiparameter surface plasmon resonance (MP-SPR) instrument SPR Navi 210 A (BioNavis Ltd., Tampere, Finland), equipped with a 785 nm laser was used. A basic piranha solution (30% H_2O_2 and 35% NH_4OH 1:1) was first used to clean SPR gold substrates (SPR102 AU, BioNavis) by heating them at 60 °C for 10 min. For PEI adsorption, a 2 mg/mL solution at pH 8.5 was injected and incubated for 10 min while SPR angular scans were recorded. After reaching signal stabilization, 3 successive washes were performed with Milli-Q water. For the adsorption of the CD enzyme, a solution of 1 mg/mL CD in 0.1 mM HEPES 10 mM KCl pH 7.4 was injected and incubated for 30 min, subsequently 3 washes were performed with Milli-Q water. The adsorption of PEI and CD was repeated up to build 3 bilayers. The adsorption of the protective coating was carried

out by injecting a 1 mg/mL PDADMAC 10 mM KCl solution and incubated for 10 min. Subsequently, a 1 mg/mL PSS 10 mM KCl solution was injected and incubated for 10 min. Among polyelectrolytes injections, three Milli-Q water rinses were performed as washing step. The same procedure was repeated for each PDADMAC/PSS bilayer.

The deposited mass density was estimated from the change in the minimum reflectance angle using the following equation [41]:

$$\Gamma = \frac{\Delta\theta Kd}{dn/dc} \quad (1)$$

where *Kd* is an instrument constant, being $Kd = 1.9 \times 10^{-7}$. A *dn/dc* value of 0.177 cm^3/g was also considered for the enzyme [42].

2.6. Measurements in Simulated Urine

Drain-source (I_{DS}) current measurements as a function of gate potential (characteristic curves, I_{DS}–V_G) were performed for a range of 25–100 µM Crn in a 1/1000 simulated urine solution (simulated urine: 392.7 mM urea, 1.13 mM KH_2PO_4, 62.34 mM $NaCO_3$) using a constant V_{DS} value of 50 mV. The V_G was scanned at 10 mV s^{-1}.

3. Results and Discussion

The rGO FETs fabrication was carried out using reduced graphene oxide via a previously established scalable solution-processing method, which reliably yields high-performance transistors compatible with standard microchip and Micro-Electro-Mechanical Systems fabrication. In contrast to CVD-grown graphene, rGO is substantially easier and cheaper to scale and enables high manufacturing yields (~98%) without the transfer-related defects and contamination typical of CVD processes. While no medical diagnostic products based on this sensor class have yet reached the market, recent progress—including the use of related devices in clinical studies—indicates that graphene-based biosensing technologies are rapidly advancing toward translational feasibility and commercial deployment. The devices exhibited an average resistance of 222 Ω (SD = 71 Ω) and a high transconductance, reaching 10.5 mS/V in the hole branch and −11.7 mS/V in the electron branch. A complete (electrochemical and morphological) characterization of the rGO FETs was previously reported where high sensitivity to pH changes were demonstrated, highlighting the feasibility of developing biosensors from these rGO FETs [43]. In particular, the pH-responsiveness enables the possibility of employing enzymes as elements of specific analyte (substrate) recognition, which in turn induce local pH changes as a consequence of their catalytic activity, thereby promoting the generation of a sensing signal that can be transduced through the transistor response.

As mentioned above, the enzymatic determination of creatinine has emerged as a potential alternative for biodetection. However, many of these systems require more than one enzymatic step using a combination of enzymes. Furthermore, in some cases, spectrophotometric quantification is required as the final quantification step [11,44,45]. On the other hand, in this work, the enzyme creatinine deiminase was used as a single enzyme system, adding ease to the construction of the biosensors. Creatinine deiminase catalyzes the hydrolysis of creatinine (Crn) into N-methylhydantoin and ammonia in the presence of water [38], as shown in Figure 1, thus generating these local pH changes on the graphene surface, which could be subsequently used to determine creatinine concentration.

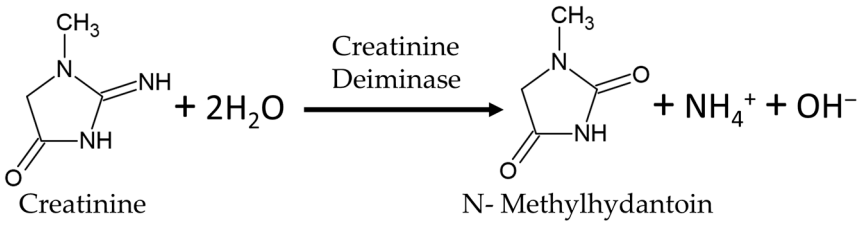


Figure 1. Enzymatic reaction of creatinine deiminase with creatinine and water.

3.1. Construction of rGO FET Biosensors for Creatinine Detection

As explained before, LbL assembly was used as an immobilization technique for creatinine deiminase (CD) integration on the semiconductor rGO channel. The LbL assembly process is schematized in Figure 2. First, the surface of rGO FETs is modified with sodium 1-pyrenesulfonate (SPS) to confer a negative charge to the graphene surface, as a charged surface is required to initiate LbL assembly. SPS molecules bind to the graphene surface through π-π interactions by their pyrene groups. Furthermore, the sulfonate groups of SPS confer a negative charge at pH > 2 [46], which is used as a basis for LbL nanoconstruction. Following SPS functionalization, PEI, a polycation, is deposited mainly due to the electrostatic interactions from the charged nitrogen moieties at pH below 9 [47]. PEI adsorption reverses the surface charge due to its large number of branches and protonated amino groups exposed on the surface. However, with increasing pH, both the degree of protonation of its amino groups and the surface charge density decrease. This generates a p-doping effect (OH^- adsorption). In this context, PEI plays an important role as a building block for LbL and as a transducer that increases sensitivity to pH changes [16,19].

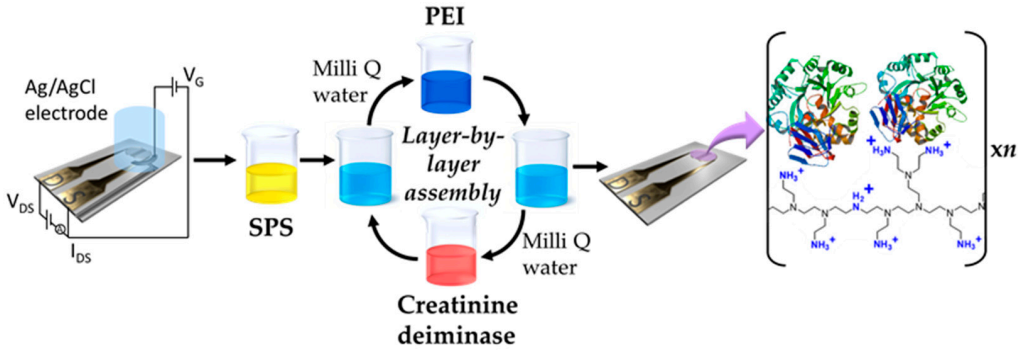


Figure 2. Schematic representation of the $(PEI/CD)_n$ LbL assembly on the rGO FETs.

One of the advantages of LbL assembly is that it does not require the formation of covalent bonds, which could affect the functionality of the immobilized enzyme if essential groups of the enzyme were involved in the covalent bond [31,48]. Furthermore, the immobilization of the covalent bond on the graphene surface could generate defects in the sp^2 lattice that would hinder the graphene's charge transport [32,33]. For these reasons, creatinine deiminase was also immobilized through electrostatic interactions using the LbL strategy. To achieve this, a CD solution at a pH above its pI (~4.3) was used, thus presenting a predominantly negative charge in the pH range that preserves its catalytic activity and stability (pH ~7–10). This negative charge is primarily due to the presence of carboxyl groups on residual amino acids such as glutamic acid and aspartic acid [49,50]. Therefore, the PEI layer on rGO FETs allows anchoring the CD enzyme to the graphene semiconductor channel. Furthermore, previous studies have shown that the PEI/CD complex helps stabilize and maintain the enzyme's native structure in the LbL assembly [50,51].

As these biosensors are based on the detection of small pH changes caused by the enzymatic reaction, the characteristic transfer curves (I_{DS} vs. V_G) of rGO FETs at different

pH values have been extensively studied [19,30]. The application of an external potential (V_G) promotes changes in the I_{DS} current since it modifies the charge carriers of the rGO. In rGO FETs in particular, a parabolic-shaped transfer curve is observed, in which the point of minimum conductivity is called the Dirac potential or inversion voltage (V_i). At V_i, a change in the nature of charge carriers is generated. For V_G more negative than V_i ($V_G < V_i$), the charge carriers are mostly holes, and at V_G values more positive than V_i, the charge carriers are electrons ($V_G > V_i$) [19]. V_i has been shown to increase as a function of pH with a linear behavior [16,19].

The response of rGO FET SPS/PEI to different Crn concentrations prior to CD immobilization was firstly examined. As seen in Figure S1 (Support Information, SI), small changes in current are observed with increasing Crn concentrations. This may be due to the adsorption of organic molecules onto the graphene surface, thereby generating changes in the mobility of charge carriers or in their conductivity [52]. However, this variation in the transfer curves can be considered insignificant compared to the response obtained for transistors modified with more than one enzyme layer in the presence of Crn (Figure 3A). When comparing the changes in V_i with increasing Crn concentrations for rGO FET SPS/PEI versus rGO FETs $(PEI/CD)_1$ (Figures 3B and S1B), slopes of 9.61 ± 1.93 and 13.29 ± 0.70 mV/Crn were obtained respectively; thus, no significant changes were observed. This may be due to the desorption of the enzyme in the first layer resulting in similar responses in the presence of Crn.

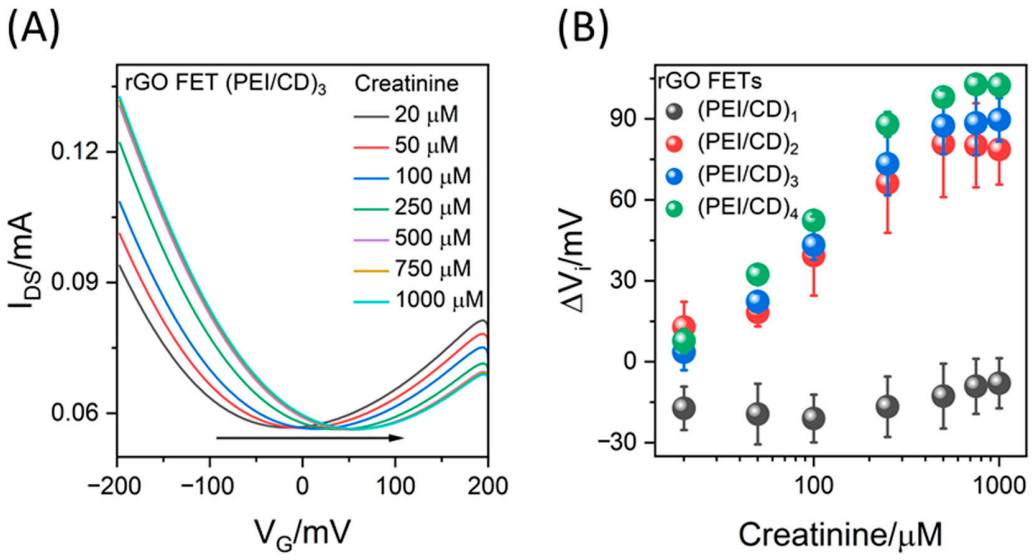


Figure 3. (**A**) Characteristic transfer curves for a rGO FET $(PEI\text{-}CD)_3$ varying the creatinine concentration from 20 to 1000 µM obtained at a V_{DS} = 50 mV in a solution of buffer 0.1 mM HEPES 10 mM KCl, pH 7.4. The arrow shows the direction of the increase in Vi. (**B**) Comparison of the change in ΔV_i as a function of creatinine concentration for rGO FETs modified with $(PEI/CD)_n$, where n ranges from 1 to 4. Error bars correspond to the SD of measurements for two FETs.

One of the advantages of the LbL surface functionalization procedure is that the amount of active material deposited can be easily tuned by increasing the number of deposition cycles, thereby augmenting the number of enzyme–polyelectrolyte bilayers. In this context, an important parameter to be optimized in the development of biosensors is the number of assembly cycles. To explore the effect of this variable, $(PEI/CD)_n$ bilayers were deposited on the rGO FETs SPS, where n represents the number of bilayers deposited on the LbL. Figure 3A shows the transfer characteristics curves for the assembly with n = 3. The response of n = 1, 2 and 4 is presented in the SI file (Section S2). A significant improvement in the response and sensitivity to Crn was observed when the assembly increased from

$(PEI/CD)_1$ to $(PEI/CD)_2$. This is clearly shown in Figure 3B, which compares V_i as a function of Crn concentration for transistors with n = 1, 2, 3 and 4 bilayers.

To account for the marked increase in sensitivity observed with the deposition of two bilayers, we also examined an intermediate configuration in which only a single PEI layer was deposited on top of the first bilayer; that is, the response of a rGO FET SPS/PEI/CD/PEI was studied. This FET showed no significant increase in response to different Crn concentrations (Section S3). Although the V_i potentials as a function of Crn concentration exhibit a shift of approximately 10 mV to more positive potentials, they keep the similar sensitivity to Crn (10.87 ± 1.04 mV/decade Crn) (Figure S3). This result allows us to state that the increase in sensitivity upon moving to two bilayers is not attributable to the PEI component. Moreover, the successive deposition of PEI onto the CD layer neither causes enzyme desorption nor leads to a decrease in its activity.

On the other hand, when increasing from one to two bilayers, the response of rGO FETs $(PEI/CD)_n$ with $n < 2$ is clearly dependent on the substrate concentration (Figures 3A and S2) as the characteristic curves shift to higher V_G values for increasing creatinine concentrations. This response is better analyzed in terms of the shift in the Dirac potential (Figure 3B). The linear shift of the ΔV_i is consistent with changes observed with increasing pH [19,30], where ΔV_i is the V_i minus the blank, V_i belonging to a 0.1 mM HEPES 10 mM KCl pH 7.4 buffer solution. Therefore, these results indicate that the CD enzyme efficiently catalyzed the hydrolysis of Crn, producing N-methylhydantoin and ammonia (Figure 1) [38]. The NH_3 molecules released by the enzymatic reaction participate in an acid-base equilibrium since they generate OH^-, thus inducing local increases in pH [11]. For rGO FETs $(PEI/CD)_2$, the sensitivity rises from 13.29 ± 0.70 mV/decade Crn for rGO FETs $(PEI/CD)_1$ to 49.15 ± 11.03 mV/decade Crn within the 20–500 µM range. The responses of transistors modified with three and four bilayers were also investigated (Figure 3B and Section S2). In this regard, rGO FETs $(PEI/CD)_3$ showed a slope of 62.66 ± 4.23 mV/decade Crn (R^2 = 0.98), whereas the rGO FETs $(PEI/CD)_4$ showed a slope of 66.54 ± 3.52 mV/decade Crn (R^2 = 0.99). Although an increase in sensitivity is observed, as shown in Figure 3B, these improvements are relatively small when moving from three to four bilayers. For this reason, and in order to minimize the preparation time of the transistors, it was determined that the optimal number of bilayers is three. Subsequent studies were therefore carried out using this configuration.

3.2. Reproducibility, Selectivity, and Stability

The response of the rGO FETs $(PEI/CD)_3$ was further studied for determining their reproducibility, selectivity, and stability. For this purpose, transfer curves from 20 to 1000 µM of Crn were performed for 7 transistors, which showed a relative standard deviation of 2.5% for Crn sensitivity, indicating very good biosensor-to-biosensor reproducibility. This can be seen in SI (Section S4).

Furthermore, to study the stability, transfer curves were measured for two biosensors on different days after synthesis (day 0 = day of synthesis). When analyzing the response in terms of V_i as a function of Crn concentration, good long-term stability was observed, with 82% of the original response retained after 10 days of storage in 0.1 mM HEPES 10 mM KCl buffer at 4 °C (Figure 4A and Section S5). The selectivity of the biosensors was studied with various interfering agents, including ascorbic acid (AA), alanine (Ala), glucose (Glu), and urea. The transistors showed a shift in the V_i to lower V_G values compared with the changes induced by Crn at similar concentrations (Figure 4B and Section S6), indicating the excellent selectivity of the rGO FETs $(PEI/CD)_3$ sensors.

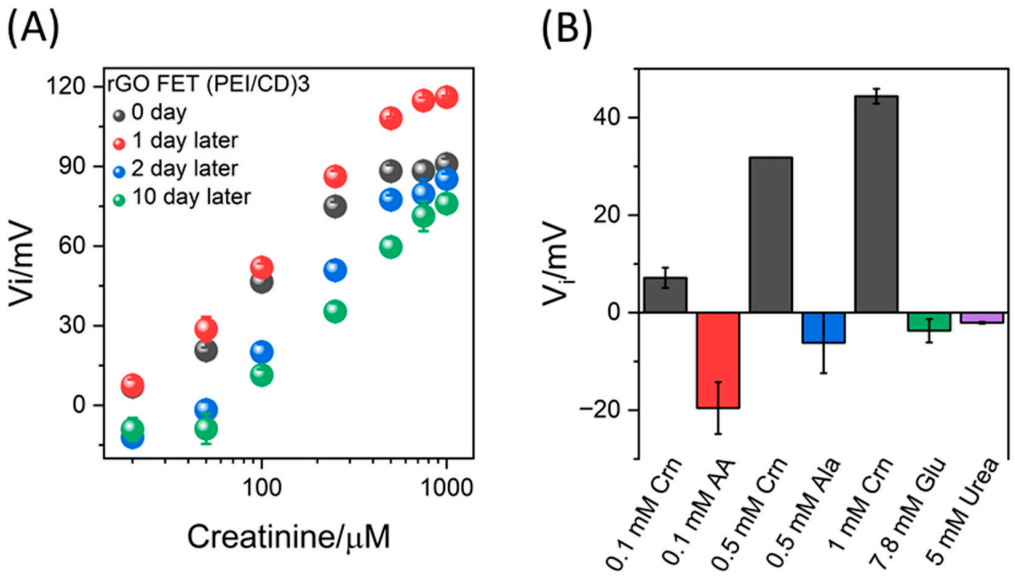


Figure 4. (**A**) Comparison of the change in ΔV_i as a function of creatinine concentration for two rGO FETs $(PEI\text{-}CD)_3$ measured 0, 1, 2, and 10 days after biosensor synthesis. Bars correspond to the SD of two sensors. (**B**) Comparison of the Dirac potential (V_i) at different creatinine concentrations for two rGO FETs $(PEI\text{-}CD)_3$ in comparison with the response observed in the presence of some interfering species: 0.1 mM ascorbic acid, 0.5 mM alanine, 7.8 mM glucose and 5 mM urea. Error bars correspond to the SD of measurements for two FETs.

3.3. Incorporation of Protective Coating

Although the sensors exhibit very good temporal stability, we also explored the incorporation of a coating that would enable measurements to be performed in more complex media. In this regard, the stability of the LbL assembly has been shown to be improved by depositing a protective coating over the LbL assembly [53–55]. We therefore deposited a PDADMAC/PSS multilayer onto rGO FETs $(PEI/CD)_3$ to improve the mechanical stability of the enzyme assembly) (Figure 5A). This protective layer consisted of three PDADMAC/PSS bilayers prepared by alternating adsorption of the polycation (PDADMAC) and the polyanion (PSS). Previous work has shown that the use of a protective layer decreases the probability of LbL assembly degradation by ~95% [55]. Such multilayers are well established to form highly stable polyelectrolyte coatings. The protection mechanism is therefore mainly mechanical in nature: by covering the enzyme-containing assembly with a stable overlayer, the likelihood of enzyme desorption or leaching into the solution is reduced. Preventing such losses is important because partial enzyme release could compromise the long-term activity and reproducibility of the sensor.

We evaluated the response of two rGO FETs $(PEI/CCD)_3(PDADMAC/PSS)_3$ to Crn concentrations from 20 to 2000 μM. The changes in the ΔV_i potential as a function of Crn concentration for these transistors can be observed in Figure 5B. The addition of the protective coating yields a sensitivity of 42.78 ± 4.07 mV/decade of Crn, which represents a decrease with respect to rGO FETs $(PEI/CD)_3$ (62.66 ± 4.23 mV/decade of Crn). This could be due to difficulties in diffusing through the protective coating and reaching the enzyme layers.

We have also checked that the addition of the protective coating does not modify the selectivity of the sensor response (Section S7). Moreover, these assemblies yield good operational stability and reproducibility when measuring successive solutions (C). Furthermore, as the purpose of these biosensors is to measure Crn concentration in biological media, we next tested six coated rGO FETs in 1/1000 simulated urine, studying their response to 25–100 μM Crn (Figure 5C). A clear decrease in sensitivity is observed, from 22.23 mV/decade for Crn

in HEPES (for six rGO FETs $(PEI/CD)_3(PDADMAC/PSS)_3$ at 25–100 µM Crn, Section S9) to 11.71 mV/decade for Crn in a 1/1000 simulated urine solution.

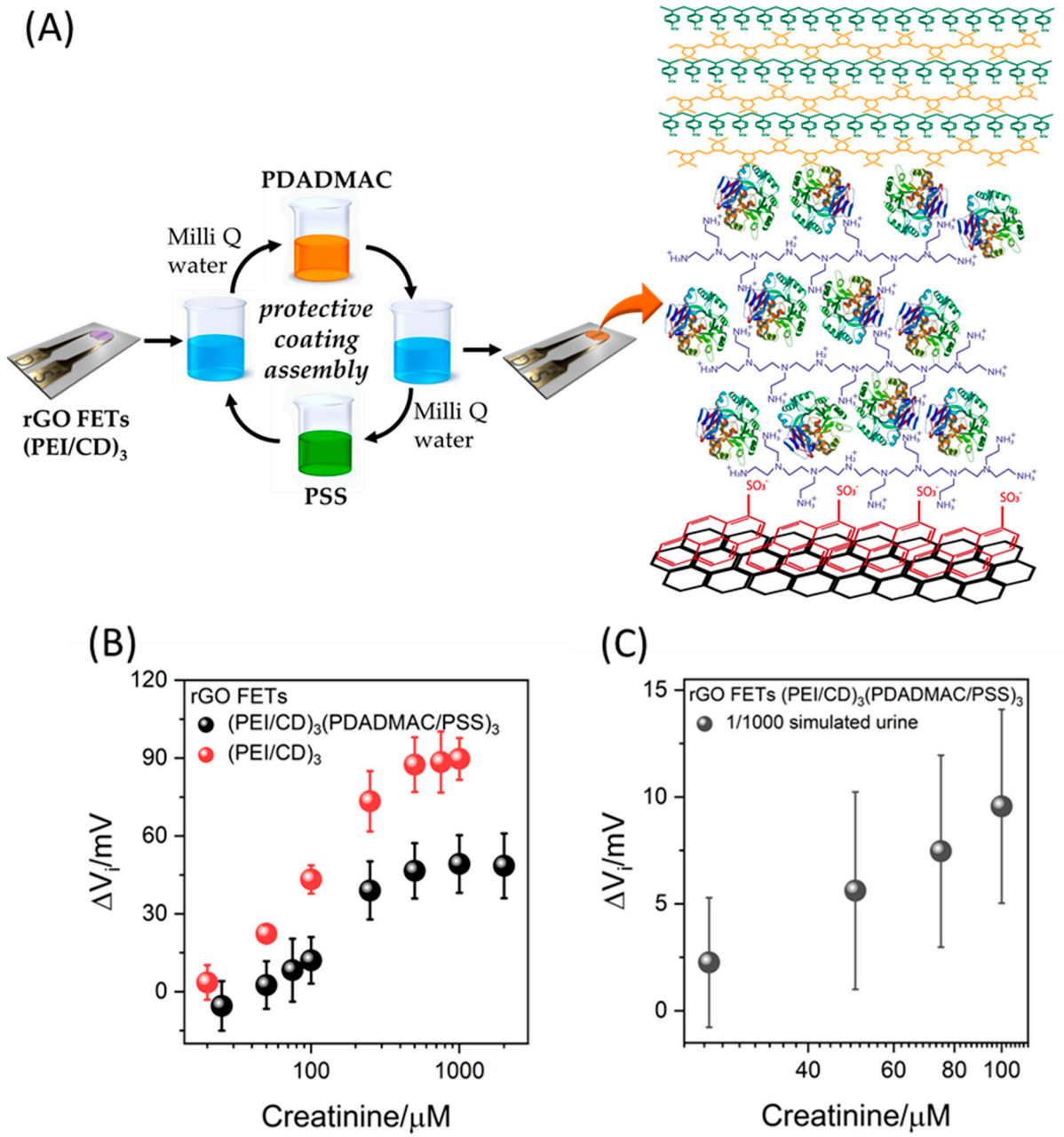


Figure 5. (**A**) Schematic representation of the assembly of the protective coating of the rGO FETs $(PEI/CD)_3$. (**B**) Comparison of the change in Dirac potential (ΔV_i) as a function of creatinine concentration for two rGO FETs $(PEI/CD)_3$ vs. two rGO FETs $(PEI/CD)_3(PDADMAC/PSS)_3$ obtained at a V_{DS} = 50 mV in buffer 0.1 mM HEPES 10 mM KCl pH 7.4. (**C**) Variation of Dirac potential (ΔV_i) at different creatinine concentrations from 25 to 100 µM in 1/1000 dilution of simulated urine obtained for 6 biosensors at a V_{DS} = 50 mV.

This decrease in sensitivity is expected, since the response of electrolyte-gated transistors depends not only on the ionic strength of the solution but also on the nature of the ionic species, as some of them may present specific interactions with the chemical groups in the coatings [38,56]. On the other hand, in complex media such as this one, there is a certain buffering capacity that can reduce the amplitude of the response, as it relies on local pH changes.

3.4. SPR Study of the Assemblies

SPR measurements were carried out to confirm the formation of the LbL $(PEI/CD)_3$ and the protective coating $(PDADMAC/PSS)_3$ (Sections S10 and S11). In Figure 6A, the changes in the angular scan curves after the injection of the first PEI and CD layers are shown. The shift of the minimum reflectance towards higher values is indicative of the adsorption of macromolecules onto the sensor surface. The adsorbed mass can be more accurately monitored by analyzing the temporal evolution of $\Delta\theta$ as each component is injected into the cell, as shown in the sensorgram in Figure 6B, as the total change in the internal reflection angle (θ_{tir}) is subtracted from the minimum reflectance angle θ_{min} to eliminate bulk refractive index variations ($\Delta\theta = \theta_{min} - \theta_{tir}$). After rinsing with Milli-Q water after each incubation, no significant changes in the SPR signal were observed, demonstrating the stability of the assembly. The as-deposited mass density was estimated from the change in the SPR signal all CD layers by applying Equation (1), obtaining values of 487.5 ng/cm^2 for the first CD layer, and 1053.5 and 1666.5 ng/cm^2 for the second and third CD layers. As shown, the total protein adsorption is not linear on the number of deposition cycles, but a supralinear growth of the LbL is observed. This result would explain the significant improvement in the response to Crn when the number of bilayers $(PEI/CD)_n$ increased from 1 to 2. This increase in the deposited mass density as the CD layers increase may be due to the strong adsorption through electrostatic interactions with the PEI molecules. Furthermore, as mentioned above, PEI molecules help to stabilize and maintain the native structure of the CD [50,51].

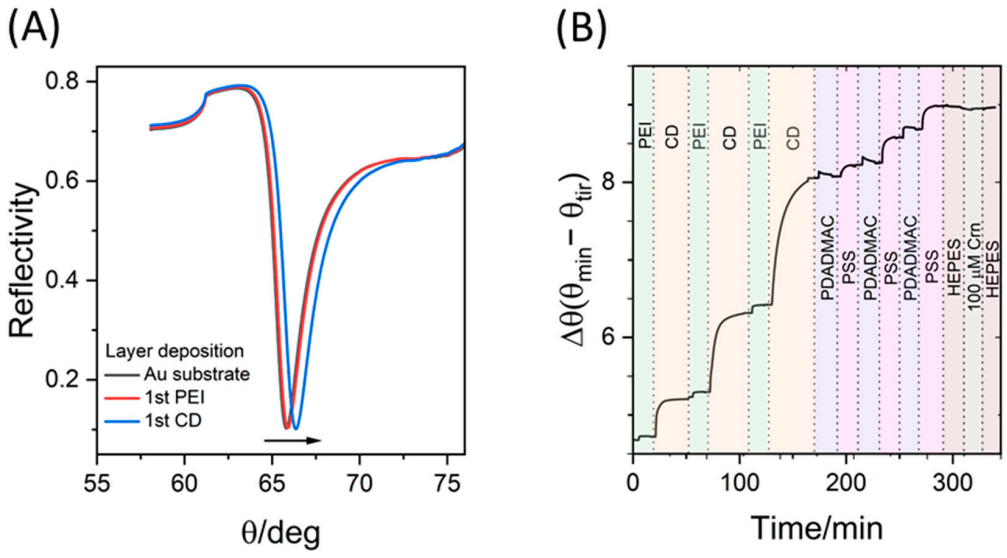


Figure 6. (**A**) SPR reflectivity curves of the first bilayer (PEI/CD) on the gold substrate. (**B**) Real-time change of the SPR $\Delta\theta(\theta_{min} - \theta_{tir})$ signal during the deposition of the LbL assembly and the assembly of the protective coating.

After verifying the assembly of the enzyme, we also monitored by SPR the assembly of the protective coating. As shown in the sensorgram (Figure 6B), the alternating injection of PDADMAC and PSS leads to an increase in the signal, thereby confirming the incorporation of this LbL assembly onto the enzyme-containing coating. Similar to the enzyme assembly, Milli-Q water was injected between the polyelectrolyte injections to perform washing steps. Finally, SPR was also employed to assess the stability of the complete supramolecular assembly under creatinine sensing conditions relevant to the rGO FET. For this purpose, buffer, a 100 μM creatinine solution (injected for several minutes), and buffer again were sequentially introduced. The preservation of the signal throughout all injections indicates

that the complete assembly remains stable under the operational conditions used for transistor measurements.

3.5. Comparison with Other Creatinine Detection Methods

As mentioned previously, enzymatic systems for creatinine detection, commonly used in point-of-care (POC) tests [1,10–12], leverage the inherent selectivity of enzymatic recognition processes to enable the development of robust detection methodologies. However, they generally require several enzymatic reaction steps before creatinine can be quantified, either by spectrophotometry or by a potentiometric sensor selective for NH_3, NH_4^+, or pH changes [11,44,45]. The latter approach relies on materials that are sensitive to pH variations due to their chemical, physical, or electronic properties [57].

As shown in Table 1, our device exhibits higher sensitivity than other transistors that employ CD as a recognition element. However, its sensitivity remains lower than that of multi-enzyme systems. On the other hand, it is important to note that our transistor requires only a single enzymatic reaction step to determine creatinine concentration, whereas multilayer devices require several such steps, which not only complicates analyte quantification but also the fabrication of these devices.

Table 1. Comparison of different biosensors that use enzymes to detect creatinine. CA = creatinine amidohydrolase, CI = creatine amidinohydrolase, SOx = sarcosine oxidase and CD = creatinine deiminase.

Type of Diagnosis	Type of the Transistor	Immobilization Method	Enzymes	Linear/ Calibration Range	Sensitivity	Ref.
Molecularly imprinted polymers	ISFET	EVAL/DMSO and creatinine on the ISFET	-	12–500 µM	-	[58]
NH_4^+ sensitive	ISFET	Covalent	CA/CI/Urease	0–20,000 µM	55 mV/pH	[59]
H_2O_2 sensitive	AuNP/Calix arene	Covalent	CA/CI/SOx	5–1000 µM	65 mV/pA	[60]
pH-sensitive FETs	MOSFET	UV-photopolymerization	CD	2–2000 µM	40 mV/pH	[61]
pH-sensitive FETs	silicalite-coated pH-FET	Covalent	CD	5–2000 µM	40 mV/pH	[62]
pH-sensitive FETs	rGO FET	LbL	CD	20–500 µM	42.78 ± 4.07 mV/decade	this work

To further contextualize the performance of our system, it is useful to compare the overall analysis time with that of standard commercial assays. A commercial creatinine assay kit (Sigma-Aldrich, Darmstadt, Germany; product number: MAK494), based on colorimetric or fluorometric detection, requires 60 min of incubation before measurement, not including the time needed for data acquisition. In contrast, our device requires only 5 min of incubation. The acquisition of each calibration point—consisting of three consecutive I_{DS}–V_G scans—takes approximately 3 min, while solution exchange and rinsing between concentrations add an additional 2 min. Including a 5-min incubation prior to each measurement, the full calibration curve (four concentration points) can be completed in approximately 40 min, and the quantification of an unknown sample within 60 min. This comparison highlights the significantly faster analysis enabled by our platform.

Moreover, rGO FETs inherently address several key challenges associated with POC deployment [39]. Their microelectrode-based geometry is compatible with low-cost polymeric encapsulation and single-use cartridge formats, while the non-covalent LbL biofunctionalization enables reagent-efficient and scalable fabrication without the need for specialized lithographic processes. Fouling resistance and mechanical stability are further enhanced by the (PDADMAC/PSS) protective multilayer, which minimizes enzymatic desorption and

helps maintain device performance in diluted complex media. Importantly, the platform preserves sensitivity in minimally processed urine and enables accurate creatinine quantification via standard addition, demonstrating robustness against variability in ionic strength and buffering conditions [63–65]. Although the device is not yet a fully integrated POC system, its architecture is intrinsically suited for real-world implementation.

4. Conclusions

In this work, we describe the development of functionalized rGO FETs using an LbL assembly for creatinine sensing. The enzyme creatinine deiminase (CD) was used as the recognition element, which was integrated into the rGO surface through electrostatic adsorption mediated by the cationic polyelectrolyte PEI. This strategy not only enabled the immobilization of CD while preserving its structural and functional properties, but also took advantage of the local pH changes caused by the enzymatic activity to produce the sensing response. As the number of LbL layers increased, enzyme deposition increased in a supralinear fashion, leading to a significant enhancement in the response to Crn. These transistors exhibited good stability and selectivity. Furthermore, in the presence of Crn, they exhibited a Dirac potential shift (V_i) resulting from the local pH change on the graphene surface produced by Crn hydrolysis. Finally, the rGO FETs $(PEI/CD)_3(PDADMAC/PSS)_3$ were able to determine the Crn concentration in a diluted simulated urine sample, demonstrating the potential of these transistors for real samples. These results not only demonstrate the capacity of LbL assemblies to advance the development of nanoconstructions for the development of sensors of clinical interest. Thus, we believe that our strategy could expand by using other recognition elements (such as antibodies or nanobodies, aptamers, proteins, ionophores, among others), provided they are compatible for LbL assembly.

Supplementary Materials: The following supporting information can be downloaded at: https://www.mdpi.com/article/10.3390/chemosensors14010003/s1, Figure S1: Characteristic transfer curves of rGO FET SPS/PEI; Figure S2: Characteristic transfer curves of transistors according to the number of bilayers $(PEI/CD)_n$; Figure S3: Response of rGO FET SPS/PEI/CD/PEI; Figure S4: Biosensor-to-biosensor reproducibility study; Figure S5: Characteristic transfer curves for an rGO FET $(PEI/CD)_3$ in the stability study; Figure S6: Characteristic transfer curves for an rGO FET $(PEI/CD)_3$ in the study of interfering species; Figure S7: Characteristic transfer curves for an rGO FET $(PEI/CD)_3(PDADMAC/PSS)_3$ in the study of interfering species; Figure S8: Operational stability study of an rGO FET $(PEI/CD)_3(PDADMAC/PSS)_3$; Figure S9: Characteristic transfer curves and ΔVi for an rGO FET $(PEI/CD)_3(PDADMAC/PSS)_3$; Table S1: Surface Plasmon Resonance (SPR); Figure S11: SPR reflectivity curves for the entire LbL assembly.

Author Contributions: Conceptualization, E.P., O.A. and W.A.M.; methodology, M.L.C.; formal analysis, M.L.C.; investigation, M.L.C. and E.P.; writing—original draft preparation, M.L.C.; writing—review and editing, E.P., O.A. and W.A.M.; visualization, M.L.C.; supervision, O.A. and W.A.M.; project administration, O.A. and W.A.M.; funding acquisition, O.A. and W.A.M. All authors have read and agreed to the published version of the manuscript.

Funding: The authors acknowledge the financial support from Universidad Nacional de La Plata (PPID-X1016) and ANPCYT (PICT 2018-04684, PICT-2020-SERIEA-02468).

Data Availability Statement: The original contributions presented in this study are included in the article/Supplementary Materials. Further inquiries can be directed to the corresponding authors.

Acknowledgments: M.L.C. acknowledges CONICET and FONCyT for scholarships. E.P., O.A. and W.A.M. are staff members of CONICET.

Conflicts of Interest: E.P., W.A.M. and O.A. are scientific advisors of GISENS BIOTECH through a cooperation agreement between UNLP, CONICET and GISENS BIOTECH (700-2845/20-000). The rest of authors declare no competing interests.

Abbreviations

The following abbreviations are used in this manuscript:

rGO FETs	reduced graphene oxide-based field-effect transistors
CD	Creatinine deiminase
Crn	Creatinine
PEI	Poly(ethylenimine)
PDADMAC	Poly(diallyldimethylammonium chloride)
PSS	Poly(4-styrenesulfonate) sodium
SPR	Surface Plasmon Resonance

References

1. Augustin, S.M.; Deshpande, R.P.; Shanthaveeranna, G.K. To Compare Creatinine Estimation by Jaffe and Enzymatic Method. *CHRISMED J. Health Res.* **2022**, *9*, 66–70. [CrossRef]
2. Kashani, K.; Rosner, M.H.; Ostermann, M. Creatinine: From physiology to clinical application. *Eur. J. Intern. Med.* **2020**, *72*, 9–14. [CrossRef] [PubMed]
3. Cánovas, R.; Cuartero, M.; Crespo, G.A. Modern creatinine (Bio)sensing: Challenges of point-of-care platforms. *Biosens. Bioelectron.* **2019**, *130*, 110–124. [CrossRef] [PubMed]
4. Stevens, P.E.; Ahmed, S.B.; Carrero, J.J.; Foster, B.; Francis, A.; Hall, R.K.; Herrington, W.G.; Hill, G.; Inker, L.A.; Kazancıoğlu, R.; et al. KDIGO 2024 Clinical Practice Guideline for the Evaluation and Management of Chronic Kidney Disease. *Kidney Int.* **2024**, *105*, S117–S314. [CrossRef]
5. Webster, A.C.; Nagler, E.V.; Morton, R.L.; Masson, P. Chronic Kidney Disease. *Lancet* **2017**, *389*, 1238–1252. [CrossRef]
6. Zuo, Y.; Yang, Y.; Zhu, Z.; He, W.; Aydin, Z. Determination of uric acid and creatinine in human urine using hydrophilic interaction chromatography. *Talanta* **2011**, *83*, 1707–1710. [CrossRef]
7. Huang, K.; Li, M.; Li, H.; Li, M.; Jiang, Y.; Fang, X. Accurate quantification of creatinine in serum by coupling a measurement standard to extractive electrospray ionization mass spectrometry. *Sci. Rep.* **2016**, *6*, 19283. [CrossRef]
8. Welch, M.J.; Cohen, A.; Hertz, H.S.; Ng, K.J.; Schaffer, R.; Van Der Lijn, P.; White, E. Determination of serum creatinine by isotope dilution mass spectrometry as a candidate definitive method. *Anal. Chem.* **1986**, *58*, 1681–1685. [CrossRef]
9. Rakesh Kumar, R.K.; Shaikh, M.O.; Chuang, C.-H. A review of recent advances in non-enzymatic electrochemical creatinine biosensing. *Anal. Chim. Acta* **2021**, *1183*, 338748. [CrossRef]
10. Smith-Palmer, T. Clinical Analysis | Sarcosine, Creatine, and Creatinine. In *Encyclopedia of Analytical Science*; Academic Press: Cambridge, MA, USA, 2019; pp. 163–172.
11. Pundir, C.S.; Kumar, P.; Jaiwal, R. Biosensing methods for determination of creatinine: A review. *Biosens. Bioelectron.* **2019**, *126*, 707–724. [CrossRef]
12. Syme, N.R.; Stevens, K.; Stirling, C.; McMillan, D.C.; Talwar, D. Clinical and Analytical Impact of Moving from Jaffe to Enzymatic Serum Creatinine Methodology. *J. Appl. Lab. Med.* **2020**, *5*, 631–642. [CrossRef] [PubMed]
13. Alimohammadzadeh, E.; Hedley, J. Advances in Graphene Field Effect Transistors (FETs) for Amine Neurotransmitter Sensing. *Appl. Sci.* **2024**, *14*, 10109. [CrossRef]
14. Zhang, Z.; Cheng, B.; Zhang, Y. Room-Temperature Operable, Fully Recoverable Ethylene Gas Sensor via Pulsed Electric Field Modulation. *Adv. Sci.* **2025**, *12*, e2500389. [CrossRef] [PubMed]
15. Sohn, I.-Y.; Kim, D.-J.; Jung, J.-H.; Yoon, O.J.; Nguyen Thanh, T.; Tran Quang, T.; Lee, N.-E. pH sensing characteristics and biosensing application of solution-gated reduced graphene oxide field-effect transistors. *Biosens. Bioelectron.* **2013**, *45*, 70–76. [CrossRef]
16. Piccinini, E.; Fenoy, G.E.; Knoll, W.; Marmisollé, W.A.; Azzaroni, O. Polyelectrolyte-Enzyme Assemblies Integrated into Graphene Field-Effect Transistors for Biosensing Applications. In *Graphene Field-Effect Transistors*; Azzaroni, O., Knoll, W., Eds.; Wiley: Hoboken, NJ, USA, 2023; pp. 285–299.
17. Guo, S.; Dong, S. Graphene nanosheet: Synthesis, molecular engineering, thin film, hybrids, and energy and analytical applications. *Chem. Soc. Rev.* **2011**, *40*, 2644. [CrossRef]
18. Zhang, X.; Jing, Q.; Ao, S.; Schneider, G.F.; Kireev, D.; Zhang, Z.; Fu, W. Ultrasensitive Field-Effect Biosensors Enabled by the Unique Electronic Properties of Graphene. *Small* **2020**, *16*, e1902820. [CrossRef]
19. Piccinini, E.; Bliem, C.; Reiner-Rozman, C.; Battaglini, F.; Azzaroni, O.; Knoll, W. Enzyme-polyelectrolyte multilayer assemblies on reduced graphene oxide field-effect transistors for biosensing applications. *Biosens. Bioelectron.* **2017**, *92*, 661–667. [CrossRef]
20. Lee, W.H.; Park, J.; Kim, Y.; Kim, K.S.; Hong, B.H.; Cho, K. Control of Graphene Field-Effect Transistors by Interfacial Hydrophobic Self-Assembled Monolayers. *Adv. Mater.* **2011**, *23*, 3460–3464. [CrossRef]

21. Geim, A.K. Graphene: Status and Prospects. *Science* **2009**, *324*, 1530–1534. [CrossRef]
22. Fu, W.; Jiang, L.; van Geest, E.P.; Lima, L.M.C.; Schneider, G.F. Sensing at the Surface of Graphene Field-Effect Transistors. *Adv. Mater.* **2017**, *29*, 1603610. [CrossRef]
23. Seo, G.; Lee, G.; Kim, M.J.; Baek, S.-H.; Choi, M.; Ku, K.B.; Lee, C.-S.; Jun, S.; Park, D.; Kim, H.G.; et al. Rapid Detection of COVID-19 Causative Virus (SARS-CoV-2) in Human Nasopharyngeal Swab Specimens Using Field-Effect Transistor-Based Biosensor. *ACS Nano* **2020**, *14*, 5135–5142. [CrossRef] [PubMed]
24. Her, J.-L.; Pan, T.-M.; Lin, W.-Y.; Wang, K.-S.; Li, L.-J. Label-free detection of alanine aminotransferase using a graphene field-effect biosensor. *Sens. Actuators B Chem.* **2013**, *182*, 396–400. [CrossRef]
25. Kim, D.J.; Sohn, I.Y.; Jung, J.H.; Yoon, O.J.; Lee, N.E.; Park, J.S. Reduced graphene oxide field-effect transistor for label-free femtomolar protein detection. *Biosens. Bioelectron.* **2013**, *41*, 621–626. [CrossRef] [PubMed]
26. Ohno, Y.; Maehashi, K.; Matsumoto, K. Chemical and biological sensing applications based on graphene field-effect transistors. *Biosens. Bioelectron.* **2010**, *26*, 1727–1730. [CrossRef]
27. Heller, I.; Chatoor, S.; Männik, J.; Zevenbergen, M.A.G.; Dekker, C.; Lemay, S.G. Influence of electrolyte composition on liquid-gated carbon nanotube and graphene transistors. *J. Am. Chem. Soc.* **2010**, *132*, 17149–17156. [CrossRef]
28. Salvo, P.; Melai, B.; Calisi, N.; Paoletti, C.; Bellagambi, F.; Kirchhain, A.; Trivella, M.G.G.; Fuoco, R.; Di Francesco, F. Graphene-based devices for measuring pH. *Sens. Actuators B Chem.* **2018**, *256*, 976–991. [CrossRef]
29. Xue, M.; Mackin, C.; Weng, W.-H.; Zhu, J.; Luo, Y.; Luo, S.-X.L.; Lu, A.-Y.; Hempel, M.; McVay, E.; Kong, J.; et al. Integrated biosensor platform based on graphene transistor arrays for real-time high-accuracy ion sensing. *Nat. Commun.* **2022**, *13*, 5064. [CrossRef]
30. Candia, M.L.; Piccinini, E.; Azzaroni, O.; Marmisollé, W.A. Digitalization of Enzyme-Linked Immunosorbent Assay with Graphene Field-Effect Transistors (G-ELISA) for Portable Ferritin Determination. *Biosensors* **2024**, *14*, 394. [CrossRef]
31. Sheldon, R.A.; van Pelt, S. Enzyme immobilisation in biocatalysis: Why, what and how. *Chem. Soc. Rev.* **2013**, *42*, 6223–6235. [CrossRef]
32. Ramasubramaniam, A.; Selhorst, R.; Alon, H.; Barnes, M.D.; Emrick, T.; Naveh, D. Combining 2D inorganic semiconductors and organic polymers at the frontier of the hard–soft materials interface. *J. Mater. Chem. C* **2017**, *5*, 11158–11164. [CrossRef]
33. Nandanapalli, K.R.; Mudusu, D.; Lee, S. Functionalization of graphene layers and advancements in device applications. *Carbon* **2019**, *152*, 954–985. [CrossRef]
34. Zhao, S.; Caruso, F.; Dähne, L.; Decher, G.; De Geest, B.G.; Fan, J.; Feliu, N.; Gogotsi, Y.; Hammond, P.T.; Hersam, M.C.; et al. The Future of Layer-by-Layer Assembly: A Tribute to ACS Nano Associate Editor Helmuth Möhwald. *ACS Nano* **2019**, *13*, 6151–6169. [CrossRef]
35. Lisdat, F. Trends in the layer-by-layer assembly of redox proteins and enzymes in bioelectrochemistry. *Curr. Opin. Electrochem.* **2017**, *5*, 165–172. [CrossRef]
36. Berninger, T.; Bliem, C.; Piccinini, E.; Azzaroni, O.; Knoll, W. Cascading reaction of arginase and urease on a graphene-based FET for ultrasensitive, real-time detection of arginine. *Biosens. Bioelectron.* **2018**, *115*, 104–110. [CrossRef] [PubMed]
37. Feng, T.; Xie, D.; Zhao, H.; Li, G.; Xu, J.; Ren, T.; Zhu, H. Tunable transport characteristics of p-type graphene field-effect transistors by poly(ethylene imine) overlayer. *Carbon* **2014**, *77*, 424–430. [CrossRef]
38. Hernández Parra, L.M.; Laucirica, G.; Toimil-Molares, M.E.; Marmisollé, W.; Azzaroni, O. Sensing creatinine in urine via the iontronic response of enzymatic single solid-state nanochannels. *Biosens. Bioelectron.* **2025**, *268*, 116893. [CrossRef] [PubMed]
39. Albesa, S.; Giménez, E.; Piccinini, J.M.; Vizoso-Pinto, M.G.; Marmisollé, W.A.; Piccinini, E.; Azzaroni, O. Machine Learning-Augmented Graphene Transistor Biosensing: Quantitative Platform Validation and Immunotesting of Hepatitis E. *ACS Sens.* **2025**. [CrossRef]
40. Montero-Jiménez, M.; Neyra Recky, J.R.; Azzaroni, O.; Scotto, J.; Marmisollé, W.A. Simultaneous Multiparameter Detection with Organic Electrochemical Transistors-Based Biosensors. *Chemosensors* **2025**, 2025120526. [CrossRef]
41. Stenberg, E.; Persson, B.; Roos, H.; Urbaniczky, C. Quantitative determination of surface concentration of protein with surface plasmon resonance using radiolabeled proteins. *J. Colloid Interface Sci.* **1991**, *143*, 513–526. [CrossRef]
42. Zhao, H.; Brown, P.H.; Schuck, P. On the Distribution of Protein Refractive Index Increments. *Biophys. J.* **2011**, *100*, 2309–2317. [CrossRef]
43. Piccinini, E.; Fenoy, G.E.; Cantillo, A.L.; Allegretto, J.A.; Scotto, J.; Piccinini, J.M.; Marmisollé, W.A.; Azzaroni, O. Biofunctionalization of Graphene-Based FET Sensors through Heterobifunctional Nanoscaffolds: Technology Validation toward Rapid COVID-19 Diagnostics and Monitoring. *Adv. Mater. Interfaces* **2022**, *9*, 2102526. [CrossRef] [PubMed]
44. Dong, Y.; Liu, Y.; Lv, J.; Yang, L.; Cui, Y. Advancements in Amperometric Biosensing Instruments for Creatinine Detection: A Critical Review. *IEEE Trans. Instrum. Meas.* **2023**, *72*, 4006915. [CrossRef]
45. Narimani, R.; Esmaeili, M.; Rasta, S.H.; Khosroshahi, H.T.; Mobed, A. Trend in creatinine determining methods: Conventional methods to molecular-based methods. *Anal. Sci. Adv.* **2021**, *2*, 308–325. [CrossRef]

46. Parviz, D.; Das, S.; Ahmed, H.S.T.; Irin, F.; Bhattacharia, S.; Green, M.J. Dispersions of Non-Covalently Functionalized Graphene with Minimal Stabilizer. *ACS Nano* **2012**, *6*, 8857–8867. [CrossRef] [PubMed]
47. Virgen-Ortíz, J.J.; dos Santos, J.C.S.; Berenguer-Murcia, Á.; Barbosa, O.; Rodrigues, R.C.; Fernandez-Lafuente, R. Polyethylenimine: A very useful ionic polymer in the design of immobilized enzyme biocatalysts. *J. Mater. Chem. B* **2017**, *5*, 7461–7490. [CrossRef]
48. Scouten, W.H.; Luong, J.H.T.; Stephenbrown, R.; Stephen Brown, R. Enzyme or protein immobilization techniques for applications in biosensor design. *Trends Biotechnol.* **1995**, *13*, 178–185. [CrossRef]
49. Gottschalk, E.M.; Hippe, H.; Patzke, F. Creatinine deiminase (EC 3.5.4.21) from bacterium BN11: Purification, properties and applicability in a serum/urine creatinine assay. *Clin. Chim. Acta* **1991**, *204*, 223–238. [CrossRef]
50. Guisan, J.M.; Fernandez-Lorente, G.; Rocha-Martin, J.; Moreno-Gamero, D. Enzyme immobilization strategies for the design of robust and efficient biocatalysts. *Curr. Opin. Green Sustain. Chem.* **2022**, *35*, 100593. [CrossRef]
51. Argaman, O.; Ben-Barak Zelas, Z.; Fishman, A.; Rytwo, G.; Radian, A. Immobilization of aldehyde dehydrogenase on montmorillonite using polyethyleneimine as a stabilization and bridging agent. *Appl. Clay Sci.* **2021**, *212*, 106216. [CrossRef]
52. He, Q.; Sudibya, H.G.; Yin, Z.; Wu, S.; Li, H.; Boey, F.; Huang, W.; Chen, P.; Zhang, H. Micropatterns of Reduced Graphene Oxide Films: Fabrication and Sensing Applications. *Am. Chem. Soc. Nano* **2010**, *4*, 3201–3208. [CrossRef]
53. Song, J.; Jańczewski, D.; Ma, Y.; Hempenius, M.; Xu, J.; Vancso, G.J. Disassembly of redox responsive poly(ferrocenylsilane) multilayers: The effect of blocking layers, supporting electrolyte and polyion molar mass. *J. Colloid Interface Sci.* **2013**, *405*, 256–261. [CrossRef]
54. Michel, M.; Izquierdo, A.; Decher, G.; Voegel, J.-C.; Schaaf, P.; Ball, V. Layer by Layer Self-Assembled Polyelectrolyte Multilayers with Embedded Phospholipid Vesicles Obtained by Spraying: Integrity of the Vesicles. *Langmuir* **2005**, *21*, 7854–7859. [CrossRef] [PubMed]
55. Diforti, J.F.; Piccinini, E.; Allegretto, J.A.; von Bilderling, C.; Marmisollé, W.A.; Azzaroni, O. Empowering Bioelectronics with Supramolecular Nanoarchitectonics: PEDOT-Based Organic Electrochemical Transistors with Tunable Electronic Properties. *ACS Appl. Electron. Mater.* **2024**, *6*, 1211–1222. [CrossRef]
56. Montero-Jimenez, M.; Lugli-Arroyo, J.; Fenoy, G.E.; Piccinini, E.; Knoll, W.; Marmisollé, W.A.; Azzaroni, O. Transduction of Amine–Phosphate Supramolecular Interactions and Biosensing of Acetylcholine through PEDOT-Polyamine Organic Electrochemical Transistors. *ACS Appl. Mater. Interfaces* **2023**, *16*, 61419–61427. [CrossRef] [PubMed]
57. Khan, M.I.; Mukherjee, K.; Shoukat, R.; Dong, H. A review on pH sensitive materials for sensors and detection methods. *Microsyst. Technol.* **2017**, *23*, 4391–4404. [CrossRef]
58. Tsai, H.-H.; Lin, C.-F.; Juang, Y.-Z.; Wang, I.-L.; Lin, Y.-C.; Wang, R.-L.; Lin, H.-Y. Multiple type biosensors fabricated using the CMOS BioMEMS platform. *Sens. Actuators B Chem.* **2010**, *144*, 407–412. [CrossRef]
59. Premanode, B.; Toumazou, C. A novel, low power biosensor for real time monitoring of creatinine and urea in peritoneal dialysis. *Sens. Actuators B Chem.* **2007**, *120*, 732–735. [CrossRef]
60. Busono, P. Development of Amperometric Biosensor for Creatinine Detection. In *Proceedings of the 7th WACBE World Congress on Bioengineering 2015, Singapore, 6–8 July 2015*; Springer: Cham, Switzerland, 2015; Volume 52, pp. 134–137. ISBN 9783319194516.
61. Marchenko, S.V.; Kucherenko, I.S.; Soldatkin, O.O.; Soldatkin, A.P. Potentiometric Biosensor System Based on Recombinant Urease and Creatinine Deiminase for Urea and Creatinine Determination in Blood Dialysate and Serum. *Electroanalysis* **2015**, *27*, 1699–1706. [CrossRef]
62. Marchenko, S.V.; Soldatkin, O.O.; Kasap, B.O.; Kurc, B.A.; Soldatkin, A.P.; Dzyadevych, S.V. Creatinine Deiminase Adsorption onto Silicalite-Modified pH-FET for Creation of New Creatinine-Sensitive Biosensor. *Nanoscale Res. Lett.* **2016**, *11*, 173. [CrossRef]
63. Meyerhoff, M.E.; Robins, R.H. Disposable Potentiometric Ammonia Gas Sensors for Estimation of Ammonia in Blood. *Anal. Chem.* **1980**, *52*, 2383–2387. [CrossRef]
64. Bader, M. A Systematic Approach to Standard Addition Methods in Instrumental Analysis. *J. Chem. Educ.* **1980**, *57*, 703. [CrossRef]
65. Diforti, J.F.; Cunningham, T.; Zegalo, Z.; Piccinini, E.; Marmisollé, W.A.; Piccinini, J.M.; Azzaroni, O. Transforming Renal Diagnosis: Graphene-Enhanced Lab-On-a-Chip for Multiplexed Kidney Biomarker Detection in Capillary Blood. *Adv. Sens. Res.* **2024**, *3*, 2400061. [CrossRef]

Disclaimer/Publisher's Note: The statements, opinions and data contained in all publications are solely those of the individual author(s) and contributor(s) and not of MDPI and/or the editor(s). MDPI and/or the editor(s) disclaim responsibility for any injury to people or property resulting from any ideas, methods, instructions or products referred to in the content.